RSC Advances

ROYAL SOCIETY OF CHEMISTRY

www.rsc.org/advances

Fabrication of Inorganic-Organic Core-Shell Heterostructure: Novel CdS@g-C_3N_4 Nanorod Arrays for Photoelectrochemical Hydrogen Evolution

Yuangang Li*, Xiaoliang Wei, Huajing Li, Rongrong Wang, Juan Feng, Hui Yun and Anning Zhou*

TOC graphic

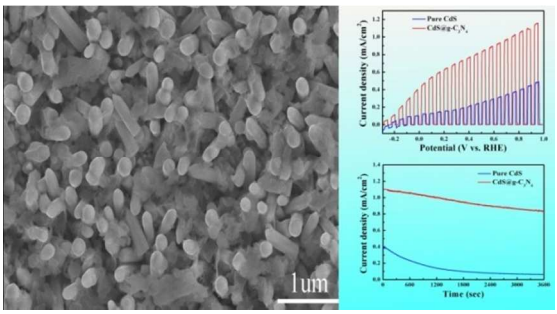

Synopsis:

Improved photoelectrochemical performance and stability have been achieved via forming heterostructured CdS@g-C_3N_4 core-shell nanorod arrays.

RSC Advances

RSCPublishing

ARTICLE

Fabrication of Inorganic-Organic Core-Shell Heterostructure: Novel CdS@g-C_3N_4 Nanorod Arrays for Photoelectrochemical Hydrogen Evolution

Cite this: DOI: 10.1039/x0xx00000x

Received 00th January 2012,
Accepted 00th January 2012

DOI: 10.1039/x0xx00000x

www.rsc.org/

Yuangang Li*, Xiaoliang Wei, Huajing Li, Rongrong Wang, Juan Feng, Hui Yun and Anning Zhou*

Novel nanoarrays composed of inorganic-organic CdS@g-C_3N_4 core-shell nanorod were fabricated via a simple hydrothermal treatment and heating process. The samples were characterized by XRD, FESEM, TEM, XPS, FTIR, UV-vis and photoelectrochemical (PEC) measurements, respectively. We find that both PEC performance and stability against light illumination of the CdS@g-C_3N_4 CSNRs are significantly enhanced compared with pure CdS NRs. The photocurrent density of the CdS@g-C_3N_4 CSNRs reaches up to 1.16 mA/cm^2, which is 2.5 times higher than that of pure CdS NRs under the same condition. More importantly, after 3600 s continuous illumination, the CdS@g-C_3N_4 CSNRs is quite stable and more than 85% of the initial photocurrent is sustained, while the photocurrent of CdS NRs decay to 20% of the initial value. Finally, a possible mechanism for the enhanced PEC performance and stability of CdS@g-C_3N_4 CSNRs heterostructure is proposed and discussed systematically based on our experimental results.

1 Introduction

Nowadays, global energy crisis and environment issues have become increasingly prominent, drawing world-wide attention. Therefore, seeking new techniques to obtain a clean and sustainable energy is very necessary.[1-3] Hydrogen evolution from water splitting using solar energy and semiconductor photocatalyst is considered to be an ideal and promising pathway.[4-8] Since Fujishima and Honda firstly reported hydrogen evolution from water splitting employing single crystal TiO_2 electrode in 1972,[9] photocatalytic hydrogen evolution from water splitting have already drawn more and more attention. Up to now, many semiconductors have been used for photochemical and photoelectrochemical (PEC) splitting of water, such as titanates, various metal oxides, sulfides, nitrides, and so on.[10, 11] Nevertheless, searching novel visible-light-responsive photocatalytic materials of low-cost, with high photocatalytic performance and chemical stability remain a big challenge.

On the other hand, nanotechnology has provided another opportunity to improve the performance of the known photocatalytic materials. For example, the activities of many photocatalysts have been significantly enhanced through nanostructuring.[12] Recently, the ordered semiconductive nanoarrays consisting of nanorods or nanowires have triggered tremendous research interest owing to its extraordinary properties, such as high length-to-diameter ratios, large surface area, direct pathway for charge transfer, and so on.[13-15] These properties can not only efficiently promote light absorption, but also enhance separation of photogenerated electron-hole pairs, especially through decoupling the length scales of charge separation and light absorption,[16-18] which would lead to significant improvement of photocatalytic activity. Moreover, these nanoarrays grown on conducting substrate can be directly used as photoelectrode in PEC system in which water reduction and oxidation half reactions can be spatially separated, avoiding the difficulty of product separation.

As an important II-VI semiconductive materials, CdS has attracted much attention and been regarded as a very promising visible-light-responsive photocatalyst for hydrogen evolution due to its relatively narrow band gap (≈ 2.4 eV) and suitable conduction band edge for reduction of H^+ to H_2.[19-22] However, the drawbacks were presented by its inherent properties, including easy aggregation resulting in reduced active surface area together with higher recombination of photogenerated electron-hole pairs, and serious photocorrosion under strong irradiation leading to the decomposition of CdS.[23, 24] Therefore, enormous efforts have been made to improve the photoactivity and stability of CdS, for instance, through coupling with other

semiconductors (TiO_2, Bi_2WO_6, NiO, Ta_2O_5, etc.),[25-28] noble metal,[29, 30] graphene,[31, 32] or polymer.[33]

Recently, an organic, metal-free polymeric photocatalyst named graphitic carbon nitrides (g-C_3N_4) has attracted extensive attention due to its unique properties, such as excellent thermal and chemical stability, and suitable band-edge position for water oxidation and reduction.[34-37] More importantly, some very recent works have already shown that coupling g-C_3N_4 with various semiconductors can efficiently improve their photocatalytic activity and stability.[38-40] Inspired by the previous works, herein, we presented a simple method to fabricate novel heterostructured CdS@g-C_3N_4 core-shell nanorod arrays (CdS@g-C_3N_4 CSNRs) on fluorine-doped tin oxide (FTO) coated glass through a hydrothermal treatment and heating process. To the best of our knowledge, this is the first report on CdS@g-C_3N_4 core-shell nanorod arrays directly grown on conducting glass substrate for PEC hydrogen evolution. Furthermore, the PEC performance and stability for hydrogen evolution of CdS nanorod arrays (CdS NRs) and CdS@g-C_3N_4 CSNRs were measured. The results indicated that the CdS@g-C_3N_4 CSNRs exhibited much higher PEC performance and better stability than pure CdS NRs.

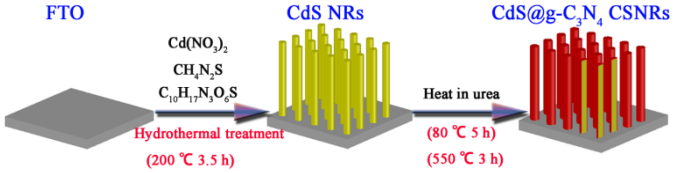

Scheme 1 A Schematic illustration for the formation process of the CdS@g-C_3N_4 CSNRs.

2 Experimental section

2.1 Materials

All reagents were analytical grade and used without further purification. Cadmium nitrate tetrahydrate ($Cd(NO_3)_2{\cdot}4H_2O$), glutathione reduced ($C_{10}H_{17}N_3O_6S$), thiourea (H_2NCSNH_2), urea ($CO(NH_2)_2$), sodium sulfite anhydrous (Na_2SO_3), sodium sulfide (Na_2S), and sodium sulfate (Na_2SO_4) were purchased from Aladdin Chemical Reagent Co., Ltd. Additionally, acetone (C_3H_6O), isopropyl alcohol (C_3H_8O), and absolute ethanol (C_2H_5OH) were bought from Sinopharm Chemical Reagent Co., Ltd. Ultrapure water was used throughout the experiment. Fluorine-doped tin oxide (FTO) coated glass with 4x1 cm^2 dimensions (8Ω/square) were obtained from Huanan Xiangcheng Technology Co., Ltd.

2.2 Preparation

The CdS@g-C_3N_4 CSNRs were fabricated on FTO substrate via a simple hydrothermal treatment and heating process, as illustrated in **Scheme 1**.

(a). Synthesis of CdS NRs: CdS NRs were grown on FTO substrate similar to the previously reported method.[41] Initially, the FTO substrate was ultrasonically cleaned in acetone, isopropyl alcohol, absolute ethanol, and ultrapure water for 15 min, respectively, and then dried using nitrogen. Subsequently, the FTO substrate was obliquely placed in a Teflon-lined stainless steel autoclave with 60 ml of aqueous solution containing cadmium nitrate, thiourea, and glutathione reduced (molar ratios 1:1:0.6, the concentration of cadmium nitrate is 16 mM), sealed and kept at 200 ^oC in an oven for 3.5 h and cooled to room temperature. The FTO substrate with CdS NRs was removed from the solution, rinsed thoroughly with absolute ethanol and ultrapure water three times, respectively, and then dried in an oven at 60 ^oC.

(b). Fabrication of CdS@g-C_3N_4 CSNRs: In a typical synthesis, 11 g of urea was added in a dried crucible with a cover. Then the FTO substrate with CdS NRs was placed in the crucible and covered with urea, which was maintained at 80 ^oC for 5 h in an oven, then at 550 ^oC for 3 h in a muffle furnace, respectively. After naturally cooling to room temperature, the FTO substrate with CdS@g-C_3N_4 CSNRs was washed thoroughly with ultrapure water several times and dried at 60 ^oC in an oven. Besides, some g-C_3N_4 powders were also obtained in the crucible.

2.3 Characterization

The crystalline structure and composition of the samples were identified with a Shimadzu7000S X-ray diffractometer (XRD) using Cu Kα (λ = 1.5418 Å) radiation at 40 kV and 30 mA in the 2θ range of 10°-80°, with a speed of 6° per minute. Scanning electron microscopy (SEM) images and energy-dispersive X-ray spectroscopy (EDX) pattern were obtained using a Hitachi S-4800 field-emission scanning electron microscopy operated at 5 kV. The optical absorption properties of the samples were measured by a Thermo Scientific Evolution 220 Ultraviolet–visible Spectrophotometer equipped with an integrating sphere using barium sulfate as the reference. Transmission electron microscopy (TEM), high-resolution transmission electron microscopy (HRTEM) observations and selected area electron diffraction (SAED) images were performed on a JEOL JEM-2100 transmission electron microscopy with an acceleration voltage of 200 kV. X-ray photoelectron spectroscopy (XPS) measurement was conducted on a Kratos Axis Ultra DLD X-ray photoelectron spectrometer with a monochromatic Al Kα (hv = 1486.69 eV) source. Infrared spectra were recorded on Nicolet Avatar 360E Fourier transform infrared (FTIR) Spectrophotometer using attenuated total reflection (ATR) measurement.

2.4 PEC measurements

All PEC tests were carried out in a classical three-electrode electrochemical workstation (CHI 660E, China) using a platinum wire, an Ag/AgCl (3 M KCl), and the CdS NRs/FTO or CdS@g-C_3N_4 CSNRs/FTO as the counter electrode, the reference electrode, and the working electrode, respectively. An aqueous solution containing 0.35 M Na_2SO_3 and 0.25 M Na_2S (pH=12) or 0.2 M Na_2SO_4 (pH=6.8) was used as electrolyte

with bubbling nitrogen for 30 min prior to measurement, which was used for all PEC tests. A 300 W xenon lamp with light intensity of (100 mW/cm^2 AM 1.5G) acted as light source during the experiment. Linear Sweep Voltammetry (LSV) was measured with a scan rate of 5 mV/s. Amperometric I-t Curves were recorded at 0.9 V versus RHE. Electrochemical impedance spectroscopy (EIS) measurement was carried out by using an AC amplitude of 20 mV in the frequency range of 1 Hz-100 kHz under open circuit potential condition. The measured potentials versus Ag/AgCl was calculated to the reversible hydrogen electrode (RHE) using the Nernst equation: $V_{RHE} = V_{Ag/AgCl} + 0.059\ pH + 0.197$.[42]

3 Results and discussion

3.1 Structure and composition characterization

XRD was employed to characterize the crystalline structure and composition of the samples. XRD patterns of pure g-C_3N_4, pure CdS NRs, and CdS@g-C_3N_4 CSNRs are shown in **Fig. 1A**. Two distinct diffraction peaks located at 27.5^o and 13.1^o are observed in the XRD pattern of pure g-C_3N_4, which can be attributed to the (002) and (100) peaks of graphitic materials and the corresponding interplanar spacing is 0.326 nm and 0.676 nm, respectively.[43] The results are consistent with the recent reports.[44, 45] With the exception of some diffraction peaks (the diffraction peaks are marked by the circle (●)) originating from the FTO substrate, pure CdS NRs display five distinguishable diffraction peaks, which are well matched with the hexagonal phase CdS (JCPDS No. 65-3414, space group: *P*63*mc*(186) with lattice parameters of a = 4.132 Å, b = 4.132 Å, and c = 6.734 Å). The peaks located at 24.8^o, 26.5^o, 28.2^o, 43.8^o, and 47.9^o correspond to (100), (002), (001), (110), (103) crystal planes of the hexagonal wurtzite CdS, respectively. As can be seen from **Fig. 1A**, the (002) peak of the CdS NRs is remarkably enhanced compared with other peaks, indicating that CdS NRs preferentially grow along the *c*-axial direction. The XRD pattern of the CdS@g-C_3N_4 CSNRs is very similar to that of pure CdS NRs. No apparent diffraction peaks of g-C_3N_4 can be detected in the XRD pattern of CdS@g-C_3N_4 CSNRs. This is probably due to low content of g-C_3N_4 in the CdS@g-C_3N_4 CSNRs and its relatively weak diffraction intensity. In addition, the characteristic peak of pure g-C_3N_4 (27.5^o) is very close to the (002) peak of CdS NRs and might overlap with each over. Same phenomenon also appeared in the reported g-C_3N_4/CdS composites.[40, 46, 47] Nevertheless, the presence of g-C_3N_4 in the CdS@g-C_3N_4 CSNRs can be easily confirmed by FTIR, XPS and EDX analyses, which will be discussed later.

In order to confirm the existence of g-C_3N_4 in the CdS@g-C_3N_4 CSNRs and study surface chemical state of the CdS@g-C_3N_4 CSNRs, XPS measurement was employed. The XPS survey spectrum (**Fig. S1**) indicates that the elements of C, N, Cd, S and small amount of O exist in the CdS@g-C_3N_4 CSNRs. **Fig. 1B-E** show high resolution XPS spectra of C 1s, N 1s, Cd 3d, and S 2p of the CdS@g-C_3N_4 CSNRs. The XPS spectrum for C 1s (**Fig. 1B**) can be separated into three peaks centered at 284.8 eV, 286.1 eV, and 288.2 eV. The peak located at 284.8 eV can be attributed to sp^2 C-C bonds, and the peak located at 288.2 eV correspond to the sp^2-bonded carbon in N-containing aromatic structure (N-C=N), which indicates the major carbon environment in the g-C_3N_4,[46, 48] The peak located at 286.1 eV could be ascribed to sp^3-bonded carbon species from the defects on g-C_3N_4 surface.[49] Three peaks centered at 398.5 eV, 399.7 eV, and 401.1 eV can be indentified from N 1s spectrum (**Fig. 1C**). The peak located at 398.5 eV is commonly ascribed to the sp^2-bonded N involved in the triazine rings (C-N=C) dominated in the g-C_3N_4. Two weak peaks located at 399.7 eV and 401.1 eV can be assigned to the tertiary N in N-(C)$_3$ units and amino groups with a hydrogen atom (C-N-H), respectively.[50, 51] In addition, the peaks of Cd 3d (**Fig. 1D**) are observed at 404.9 eV and 411.6 eV, which are attributed to Cd 3d$_{5/2}$ and Cd 3d$_{3/2}$ for Cd^{2+} in CdS.[52] Moreover, the binding energy of Cd 3d in the CdS@g-C_3N_4 CSNRs is slightly lower than those of pure CdS NRs. (**Fig. S2**) The shift of binding energy suggests interaction between CdS and g-C_3N_4.[37] The XPS spectrum for S 2p (**Fig. 1E**) shows the peaks at 161.2 eV (S 2p$_{3/2}$) and 162.4 eV (S 2p$_{1/2}$), which are ascribed to S^{2-} in CdS.[53] These results confirm that both CdS and g-C_3N_4 exist in the CdS@g-C_3N_4 CSNRs.

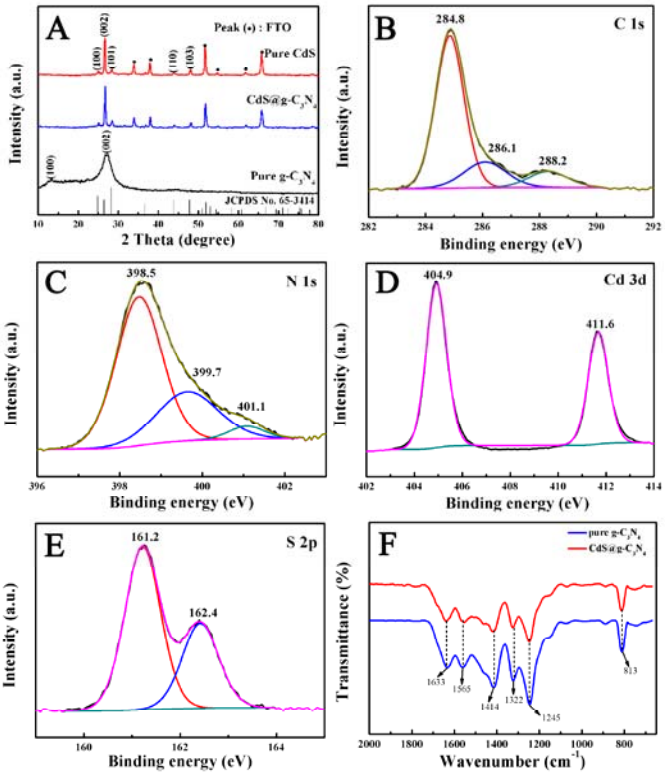

Fig. 1 (A) XRD patterns of pure g-C_3N_4, pure CdS NRs, and CdS@g-C_3N_4 CSNRs; High resolution XPS spectra of (B) C 1s, (C) N 1s, (D) Cd 3d, and (E) S 2p for the CdS@g-C_3N_4 CSNRs; (F) FTIR spectra of pure g-C_3N_4 and CdS@g-C_3N_4 CSNRs.

The existence of g-C_3N_4 in the CdS@g-C_3N_4 CSNRs was further confirmed by FTIR analysis using attenuated total reflection (ATR) measurement. **Fig. 1F** shows a comparison of

the FTIR spectra of pure g-C_3N_4 and CdS@g-C_3N_4 CSNRs. As for pure g-C_3N_4, some strong bands are observed in 1200-1650 cm^{-1} region. The peaks at about 1245, 1322, 1414, 1565, 1633 cm^{-1} are attributed to the typical stretching modes of CN heterocycles.[54] In addition, the peak located at 813 cm^{-1} correspond to characteristic breathing mode of triazine units.[55] For CdS@g-C_3N_4 CSNRs, all characteristic absorption peaks of g-C_3N_4 appear in the CdS@ g-C_3N_4 CSNRs. However, the absorption peaks of CdS are not obvious in the CdS@ g-C_3N_4 CSNRs, which could be due to the fully coverage of g-C_3N_4 over CdS. On the basis of the above results, it is further indicate that the g-C_3N_4 exist in the CdS@g-C_3N_4 CSNRs.

3.2 Morphology and microstructure analysis.

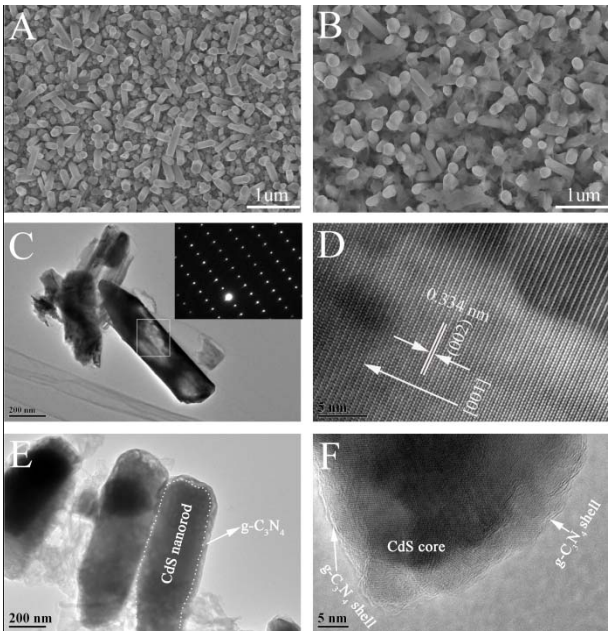

Fig. 2 Typical top-view FESEM images of (A) CdS NRs and (B) CdS@g-C_3N_4 CSNRs; TEM images of (C) CdS nanorod (the inset is its SAED pattern) and (E) CdS@g-C_3N_4 core-shell nanorod, HRTEM images of (D) CdS nanorod and (F) CdS@g-C_3N_4 core-shell nanorod.

To investigate the morphology and microstructure of the prepared samples, FESEM was done. It is observed from **Fig. 2A** that the CdS nanorods show regular hexagonal tips and the diameter of CdS nanorods is 150-200 nm. After the coating of g-C_3N_4 onto CdS nanorods, the nanostructure of the CdS nanorods was well reserved (**Fig. 2B**) and obvious film-like materials can be observed coating on the nanorods. Furthermore, the diameter of nanorods is slight increased compared with pure CdS nanorod, suggesting that the CdS@g-C_3N_4 core-shell nanorods are successfully obtained. Additionally, we can see clearly that the g-C_3N_4 display lamellar structure consisting of sheets surrounding the nanorods (**Fig. 2B**). EDX was also carried out to explore the element composition of CdS@g-C_3N_4 CSNRs. As revealed in (**Fig. S3**), the EDX spectrum of CdS@g-C_3N_4 CSNRs contains C, N, Cd, S, and Sn elements (from FTO substrate), which is in good agreement with the result of XPS analysis.

In order to acquire more detailed information about the morphology and microstructure of the prepared samples, TEM and HRTEM were performed. As shown in **Fig. 2C**, the diameter of the unbroken CdS nanorod is 200 nm, which is in agreement with the result of SEM. From the comparison of **Fig. 2C** and **Fig. 2E**, we can observe that the CdS@g-C_3N_4 nanorod exhibit a one-dimensional core-shell structure compared with original CdS nanorod, and it can be clearly seen that the g-C_3N_4 as shell are well coated on CdS nanorod. In addition, as can be seen from **Fig. 2E**, the diameter of CdS@g-C_3N_4 core-shell nanorod is slight increase compared with that of CdS nanorod (200 nm), and the g-$C_3N_4$is composed of some sheets with wrinkles and irregular shape, which is well consistent with the SEM result. The HRTEM image in **Fig. 2D** reveals clear lattice fringes of well-crystallized CdS and the spacing between the adjacent lattice fringes of along the growth direction of CdS nanorod is about 0.334nm, corresponding to the interplanar spacing of the (002) plane of CdS which is in good agreement with the results of XRD measurement. The selected area electron diffraction (SAED) pattern (the inset in **Fig. 2C**) indicates that the CdS nanorod is a single crystal. Therefore, we can confirm that CdS nanorod indeed grow along the direction of the *c*-axis. The result of the HRTEM image (**Fig. 2F**) clearly exhibits intimate interface between g-C_3N_4 shell and CdS core, indicating the formation of heterostructure between g-C_3N_4 shell and CdS core rather than a simply physical mixture, which is vital for promoting the transfer and separation of photogenerated electron-hole pairs, and therefore improving PEC performance of the CdS@g-C_3N_4 CSNRs. Combined with SEM result, the above results demonstrate that the CdS@g-C_3N_4 CSNRs were successfully achieved by a simple hydrothermal treatment and heating process.

3.3 Optical absorption properties.

The optical absorption properties of pure g-C_3N_4, pure CdS NRs and CdS@g-C_3N_4 CSNRs were identified by UV-vis diffuse reflectance spectroscopy (DRS). The normalized absorbance of the samples versus wavelength is displayed in **Fig. 3**. As can be seen from **Fig. 3**, the absorption edge for pure g-C_3N_4 is about 460 nm, which can be ascribed to band gap of ≈ 2.7 eV and is consistent with the literature value.[56] While pure CdS NRs exhibit sharp absorption edge at around 530 nm, corresponding to band gap of ≈ 2.3 eV, which is in agreement with the previous report.[57] Compared with pure g-C_3N_4 and CdS NRs, the absorption spectrum of CdS@g-C_3N_4 CSNRs assigned to both g-C_3N_4 and CdS NRs is apparent. Moreover, the CdS@g-C_3N_4 CSNRs show enhanced light absorption intensity in the 530-650 nm visible range with a red-shifted compared with pure CdS NRs, which can be attributed to interaction between CdS and g-C_3N_4.[58] Therefore, the results of UV-vis DRS suggest that formation of CdS@g-C_3N_4

heterostructure broaden its optical absorption range, which will probably enhance efficient utilization of the solar energy.

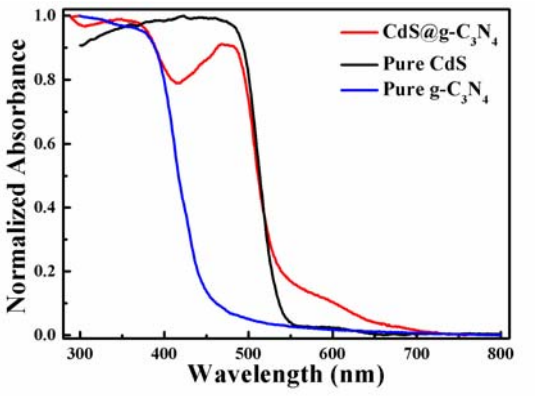

Fig. 3 UV-vis diffuse reflectance spectra of g-C_3N_4, CdS NRs and CdS@g-C_3N_4 CSNRs.

3.4 Photoelectrochemical performance

To investigate PEC properties of CdS NRs and CdS@g-C_3N_4 CSNRs, Linear Sweep Voltammetry (LSV) measurement was obtained under chopped 100 mW/cm^2 (AM 1.5G) illumination in an aqueous solution containing 0.35 M Na_2SO_3 and 0.25 M Na_2S (pH=12) with a scan rate of 5 mV/s. As described in **Fig. 4A**, with the increase of the forward bias potential, both CdS NRs and CdS@g-C_3N_4 CSNRs show increased photocurrent density, which is an indication of typical n-type semiconductor.[59] It can be clearly seen that the CdS@g-C_3N_4 CSNRs shows a enhanced photocurrent density under chopped (100 mW/cm^2 AM 1.5G) illumination compared with that of CdS NRs and reach a maximum value of about 1.16 mA/cm^2, which is 2.5 times higher than that of CdS NRs (0.46 mA/cm^2). The enhanced photocurrent density implies that more efficient charge transfer and separation is achieved, after the formation of CdS@g-C_3N_4 core-shell heterostructure.

In order to compare the stability of CdS NRs and CdS@g-C_3N_4 CSNRs, we tested the I-t curves at 0.9 V versus RHE under continuous (100 mW/cm^2 AM 1.5G) illumination for one hour using the two kinds of electrodes, respectively. As exhibited in **Fig. 4B**, the photocurrent density of CdS NRs decreased to 20% of the initial value after one hour. The decrease of photocurrent density probably results from photocorrosion, which leads to decomposition of CdS NRs.[23, 24] Notably, after g-C_3N_4 as shell coating onto CdS NRs, the photocurrent density is quite stable and still preserved about 85% of the initial photocurrent density after one hour. Apparently, the existence of g-C_3N_4 on surface of CdS NRs effectively inhibit the photocorrosion process, which indicates that the CdS@g-C_3N_4 CSNRs heterostructure can efficiently promote the transport of corrosive holes from CdS to g-C_3N_4, so improving the stability of CdS NRs. Moreover, The PEC performance and stability of pure CdS NRs and CdS@g-C_3N_4 CSNRs in a nonsacrificial system were also systematically investigated. It is found that after g-C_3N_4 coating, the PEC performance and stability of CdS NRs were greatly improved (see **Fig. S4** and **Fig. S5**).

Electrochemical impedance spectroscopy is a powerful tool to analyze charge transfer properties and separation efficiency of photogenerated charge carriers.[60, 61] In order to support the above results and clarify transfer and separation mechanism of photogenerated charge carriers, electrochemical impedance spectroscopy (Nyquist plots) was performed in an aqueous solution containing 0.35 M Na_2SO_3 and 0.25 M Na_2S (pH=12) with an AC amplitude of 20 mV under open circuit potential condition over the frequency range of 1 Hz-100 kHz. Both the obtained Nyquist plots (symbols) and the fitted plots (dotted lines) by Z-view software are listed in **Fig. 4C**. The fitted values of R_{ct} (charge transfer resistance) were 2765 Ω and 2468Ω for pure CdS NRs and CdS@g-C_3N_4 CSNRs, respectively. As presented in **Fig. 4C**, the CdS@g-C_3N_4 CSNRs show smaller arc radius as compared with pure CdS NRs. Generally speaking, a smaller arc radius on the EIS (Nyquist plots) represents a faster interfacial charge transfer and higher separation efficiency of photogenerated charge carriers.[62, 63] So the result of EIS demonstrates that CdS@g-C_3N_4 CSNR is more favorable for transfer and separation of photogenerated charge carriers compared with CdS NRs, thus enhancing PEC performance.

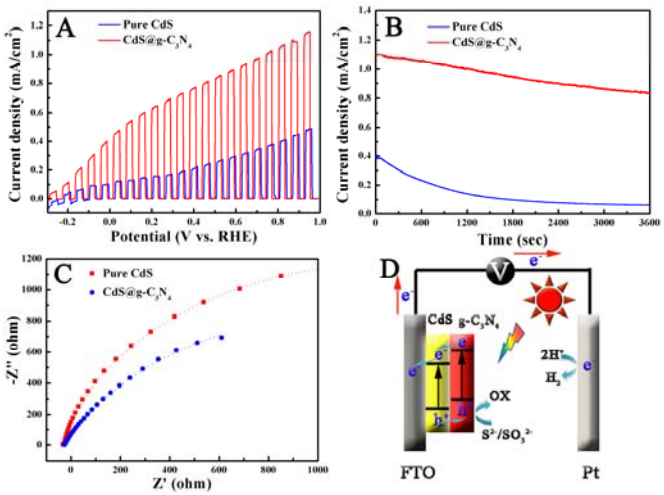

Fig. 4 (A) Photocurrent density versus potential curves for CdS NRs and CdS@g-C_3N_4 CSNRs; (B) Photostability measurements of CdS NRs and CdS@g-C_3N_4 CSNRs; (C) Electrochemical impedance spectra (Nyquist plots) for CdS NRs and CdS@g-C_3N_4 CSNRs; (D) Schematic diagram for transfer and separation of photogenerated charges in the CdS@g-C_3N_4 CSNRs heterostructure, and the process of hydrogen evolution in our PEC system based on CdS@g-C_3N_4 CSNRs.

3.5 Open circuit voltage decay measurements

To further investigated the efficient charge separation in the CdS@g-C_3N_4 CSNRs heterostructure and the lifetime of electrons, open circuit voltage decay was measured. As displayed in (**Fig. S6 and Fig. S7**), the results show that CdS@g-C_3N_4 CSNRs heterostructure alleviate open circuit voltage decay and exhibit a much higher lifetime of electrons with a lower recombination rate by the calculation of model equation [64] compared with pure CdS NRs. This phenomenon strong demonstrates that efficient charge separation is obtained in the CdS@g-C_3N_4 CSNRs heterostructure.

3.6 Mechanism analysis

On the basis of our experimental results, a possible mechanism for the enhanced PEC performance of the CdS@g-C_3N_4 CSNRs heterostructure is proposed and shown in **Fig. 4D**. It is well known that both CdS and g-C_3N_4 can produce photogenerated electrons and holes under the excitation of sunlight. Since the valance band and conduction band of g-C_3N_4 is higher than those of CdS (see **Fig. 4D**), respectively,[65, 66] a well-matched type-II heterostructure was formed.[67] Under the excitation of sunlight, the photogenerated electrons on conduction band of g-C_3N_4 can directly migrate to that of CdS, while the photogenerated holes on valance band of CdS can transfer to that of g-C_3N_4. Therefore, photogenerated electrons and holes can be efficiently separated. The PEC performance and EIS results also confirm the superior charge transfer and recombination inhibition in the CdS@g-C_3N_4 CSNRs, which support the proposed mechanism. Meanwhile, the process of hydrogen evolution in our PEC system based on CdS@g-C_3N_4 CSNRs is also depicted in **Fig. 4D**. Under the excitation of sunlight, the photogenerated electrons on conduction band of g-C_3N_4 flow to that of CdS, then to the FTO substrate, and further through the external circuit to the Pt counter electrode, finally these electrons are consumed by reducing H^+ to H_2. At the same time, the photogenerated holes on the valance band of CdS transfer to that of g-C_3N_4, which react with scavenger SO_3^{2-} and S^{2-} on the g-C_3N_4 surface.

4 Conclusions

In conclusion, we have demonstrated in the article that both the PEC performance and stability were significantly enhanced through forming core-shell nanorod arrays with g-C_3N_4 as shell coated onto the CdS nanorod. The g-C_3N_4 layer plays a dual role at the same time. It not only act as an organic semiconductor to form an inorganic-organic heterostructure with inorganic CdS, which markedly enhance PEC performance of CdS, but also as a protective layer to protect CdS from photocorrosion, which greatly improve stability of CdS. Our results provide beneficial new insight for the development of other inorganic-organic nanostructured composites with enhanced activity and stability.

Acknowledgements

We acknowledge financial support from the National Natural Science Foundation of China (21103134). We thank Kaiqiang Liu and Xiangyang Yan (School of Chemistry and Chemical Engineering, Shaanxi Normal University) for their assistance in TEM and XPS measurements.

Notes and references

College of Chemistry and Chemical Engineering, Xi'an University of Science and Technology, Xi'an 710054, China.
Tel /Fax: +86 29 85583183;
E-mail: chemliyg@gmail.com (Y. L.)； *psu564@139.com* (A. Z.)

Electronic Supplementary Information (ESI) available: XPS survey spectrum of the CdS@g-C_3N_4 CSNRs, XPS spectra of Cd for the CdS NRs and the CdS@g-C_3N_4 CSNRs, Linear Sweep Voltammetry (LSV) measurement and I-t curves of the CdS NRs and the CdS@g-C_3N_4 CSNRs, SEM and TEM of the CdS@g-C_3N_4 CSNRs, XRD pattern of blank FTO, Linear Sweep Voltammetry (LSV) measurement of pure g-C_3N_4 and different deposition times of g-C_3N_4 onto CdS NRs, Incident photon to current efficiency (IPCE), open circuit voltage decay measurements and lifetime of electron curves of CdS NRs and CdS@g-C_3N_4 CSNRs.

1. J. Wu, Y. Li, J. Kubota, K. Domen, M. Aagesen, T. Ward, A. Sanchez, R. Beanland, Y. Zhang, M. Tang, S. Hatch, A. Seeds and H. Liu, *Nano Lett.*, 2014, **14**, 2013-2018.
2. L. He, L. Jing, Y. Luan, L. Wang and H. Fu, *ACS Catal.*, 2014, **4**, 990-998.
3. Z. Huang, Z. Chen, Z. Chen, C. Lv, H. Meng and C. Zhang, *ACS Nano*, 2014, **8**, 8121-8129.
4. Z. Zou, J. Ye, K. Sayama and H. Arakawa, *Nature*, 2001, **414**, 625-627.
5. M. G. Walter, E. L. Warren, J. R. McKone, S. W. Boettcher, Q. Mi, E. A. Santori and N. S. Lewis, *Chem. Rev.*, 2010, **110**, 6446-6473.
6. Y. Tachibana, L. Vayssieres and J. R. Durrant, *Nat. Photonics*, 2012, **6**, 511-518.
7. S. Sun, W. Wang, D. Li, L. Zhang and D. Jiang, *ACS Catal.*, 2014, 3498-3503.
8. A. Kudo and Y. Miseki, *Chem. Soc. Rev.*, 2009, **38**, 253-278.
9. A. Fujishima and K. Honda, *Nature*, 1972, **238**, 37-38.
10. F. E. Osterloh, *Chem. Mater.*, 2007, **20**, 35-54.
11. M. Zhu, P. Chen and M. Liu, *ACS Nano*, 2011, **5**, 4529-4536.
12. T. M. Gür, S. F. Bent and F. B. Prinz, *J. Phys. Chem. C*, 2014, **118**, 21301-21315.
13. H. Kim, M. Seol, J. Lee and K. Yong, *J. Phys. Chem. C*, 2011, **115**, 25429-25436.
14. B. Weng, S. Liu, Z.-R. Tang and Y.-J. Xu, *RSC Advances*, 2014, **4**, 12685-12700.
15. C. X. Guo, Y. Dong, H. B. Yang and C. M. Li, *Adv. Energy Mater.*, 2013, **3**, 997-1003.
16. L. Gao, Y. Cui, J. Wang, A. Cavalli, A. Standing, T. T. T. Vu, M. A. Verheijen, J. E. M. Haverkort, E. P. A. M. Bakkers and P. H. L. Notten, *Nano Lett.*, 2014, **14**, 3715-3719.
17. H. Wang, Y. Bai, Q. Wu, W. Zhou, H. Zhang, J. Li and L. Guo, *Phys. Chem. Chem. Phys.*, 2011, **13**, 7008-7013.
18. J. Wang and W.-D. Zhang, *Electrochim. Acta*, 2012, **71**, 10-16.
19. Y. Zhang, Y. Tang, X. Liu, Z. Dong, H. H. Hng, Z. Chen, T. C. Sum and X. Chen, *Small*, 2013, **9**, 996-1002.

20. X. Chen, S. Shen, L. Guo and S. S. Mao, *Chem. Rev.*, 2010, **110**, 6503-6570.
21. Y. Li, Y. Hu, S. Peng, G. Lu and S. Li, *J. Phys. Chem. C*, 2009, **113**, 9352-9358.
22. X. Wang, C. Liow, D. Qi, B. Zhu, W. R. Leow, H. Wang, C. Xue, X. Chen and S. Li, *Adv. Mater.*, 2014, **26**, 3506-3512.
23. H. N. Kim, T. W. Kim, I. Y. Kim and S.-J. Hwang, *Adv. Funct. Mater.*, 2011, **21**, 3111-3118.
24. L. Qi, J. Yu and M. Jaroniec, *Phys. Chem. Chem. Phys.*, 2011, **13**, 8915-8923.
25. S. Qian, C. Wang, W. Liu, Y. Zhu, W. Yao and X. Lu, *J. Mater. Chem.*, 2011, **21**, 4945-4952.
26. L. Ge and J. Liu, *Appl. Catal., B*, 2011, **105**, 289-297.
27. Z. Khan, M. Khannam, N. Vinothkumar, M. De and M. Qureshi, *J. Mater. Chem.*, 2012, **22**, 12090-12095.
28. L. Xu, W. Shi and J. Guan, *Catal. Commun.*, 2012, **25**, 54-58.
29. Y. Wang, Y. Wang and R. Xu, *J. Phys. Chem. C*, 2012, **117**, 783-790.
30. L. Sheeney-Haj-Ichia, S. Pogorelova, Y. Gofer and I. Willner, *Adv. Funct. Mater.*, 2004, **14**, 416-424.
31. N. Zhang, Y. Zhang, X. Pan, X. Fu, S. Liu and Y.-J. Xu, *J. Phys. Chem. C*, 2011, **115**, 23501-23511.
32. Q. Li, B. Guo, J. Yu, J. Ran, B. Zhang, H. Yan and J. R. Gong, *J. Am. Chem. Soc.*, 2011, **133**, 10878-10884.
33. H. Zhang and Y. Zhu, *J. Phys. Chem. C*, 2010, **114**, 5822-5826.
34. X. Wang, K. Maeda, A. Thomas, K. Takanabe, G. Xin, J. M. Carlsson, K. Domen and M. Antonietti, *Nat. Mater.*, 2009, **8**, 76-80.
35. Y. Zheng, J. Liu, J. Liang, M. Jaroniec and S. Z. Qiao, *Energy Environ. Sci.*, 2012, **5**, 6717-6731.
36. Y. Wang, X. Wang and M. Antonietti, *Angew. Chem. Int. Ed.*, 2012, **51**, 68-89.
37. C. Chang, L. Zhu, S. Wang, X. Chu and L. Yue, *ACS Appl. Mater. Interfaces*, 2014, **6**, 5083-5093.
38. Y. Wang, R. Shi, J. Lin and Y. Zhu, *Energy Environ. Sci.,* 2011, **4**, 2922-2929.
39. Y. Tian, B. Chang, Z. Yang, B. Zhou, F. Xi and X. Dong, *RSC Advances*, 2014, **4**, 4187-4193.
40. J. Zhang, Y. Wang, J. Jin, J. Zhang, Z. Lin, F. Huang and J. Yu, *ACS Appl. Mater. Interfaces*, 2013, **5**, 10317-10324.
41. C. Yang, M. Li, W.-H. Zhang and C. Li, *Sol. Energy Mater. Sol. Cells*, 2013, **115**, 100-107.
42. C. Yang, Z. Wang, T. Lin, H. Yin, X. Lü, D. Wan, T. Xu, C. Zheng, J. Lin, F. Huang, X. Xie and M. Jiang, *J. Am. Chem. Soc.*, 2013, **135**, 17831-17838.
43. Z. Chen, P. Sun, B. Fan, Z. Zhang and X. Fang, *J. Phys. Chem. C*, 2014, **118**, 7801-7807.
44. Y. Zhang, J. Liu, G. Wu and W. Chen, *Nanoscale*, 2012, **4**, 5300-5303.
45. J. Liu, T. Zhang, Z. Wang, G. Dawson and W. Chen, *J. Mater. Chem.*, 2011, **21**, 14398-14401.
46. S.-W. Cao, Y.-P. Yuan, J. Fang, M. M. Shahjamali, F. Y. C. Boey, J. Barber, S. C. Joachim Loo and C. Xue, *Int. J. Hydrogen Energy*, 2013, **38**, 1258-1266.
47. M. Lu, Z. Pei, S. Weng, W. Feng, Z. Fang, Z. Zheng, M. Huang and P. Liu, *Phys. Chem. Chem. Phys.*, 2014, **16**, 21280-21288.
48. A. Vinu, *Adv. Funct. Mater.*, 2008, **18**, 816-827.
49. G. Zhang, J. Zhang, M. Zhang and X. Wang, *J. Mater. Chem.*, 2012, **22**, 8083-8091.
50. A. Thomas, A. Fischer, F. Goettmann, M. Antonietti, J.-O. Muller, R. Schlogl and J. M. Carlsson, *J. Mater. Chem.*, 2008, **18**, 4893-4908.
51. Q. Xiang, J. Yu and M. Jaroniec, *J. Phys. Chem. C*, 2011, **115**, 7355-7363.
52. F.-X. Xiao, J. Miao and B. Liu, *J. Am. Chem. Soc.*, 2014, **136**, 1559-1569.
53. L. J. Zhang, R. Zheng, S. Li, B. K. Liu, D. J. Wang, L. L. Wang and T. F. Xie, *ACS Appl. Mater. Interfaces*, 2014, **6**, 13406-13412.
54. S. C. Yan, Z. S. Li and Z. G. Zou, *Langmuir*, 2009, **25**, 10397-10401.
55. H. Xu, J. Yan, X. She, L. Xu, J. Xia, Y. Xu, Y. Song, L. Huang and H. Li, *Nanoscale*, 2014, **6**, 1406-1415.
56. F. Dong, L. Wu, Y. Sun, M. Fu, Z. Wu and S. C. Lee, *J. Mater. Chem.*, 2011, **21**, 15171-15174.
57. C. Yang, S. Liu, M. Li, X. Wang, J. Zhu, R. Chong, D. Yang, W.-H. Zhang and C. Li, *J. Colloid Interface Sci.*, 2013, **393**, 58-65.
58. L. Ge, F. Zuo, J. Liu, Q. Ma, C. Wang, D. Sun, L. Bartels and P. Feng, *J. Phys. Chem. C*, 2012, **116**, 13708-13714.
59. M. J. Natan, J. W. Thackeray and M. S. Wrighton, *J. Phys. Chem.*, 1986, **90**, 4089-4098.
60. Y. Liu, D.-P. Wang, Y.-X. Yu and W.-D. Zhang, *Int. J. Hydrogen Energy*, 2012, **37**, 9566-9575.
61. F. He, G. Chen, Y. Yu, S. Hao, Y. Zhou and Y. Zheng, *ACS Appl. Mater. Interfaces*, 2014, **6**, 7171-7179.
62. L.-W. Zhang, H.-B. Fu and Y.-F. Zhu, *Adv. Funct. Mater.*, 2008, **18**, 2180-2189.
63. Y.-X. Yu, W.-X. Ouyang, Z.-T. Liao, B.-B. Du and W.-D. Zhang, *ACS Appl. Mater. Interfaces*, 2014, **6**, 8467-8474.
64 J. H. Bang and P. V. Kamat, Adv. Funct. Mater., 2010, 20, 1970-1976.
65. R. C. Pawar, V. Khare and C. S. Lee, *Dalton Trans.*, 2014, **43**, 12514-12527.
66. J. Fu, B. Chang, Y. Tian, F. Xi and X. Dong, *J. Mater. Chem. A*, 2013, **1**, 3083-3090.
67. Y. Wang, Q. Wang, X. Zhan, F. Wang, M. Safdar and J. He, *Nanoscale*, 2013, **5**, 8326-8339.